Biomedical Optics EXPRESS

Mitochondrial redox studies of oxidative stress in kidneys from diabetic mice

Sepideh Maleki,[1] Reyhaneh Sepehr,[1] Kevin Staniszewski,[1] Nader Sheibani,[2] Christine M. Sorenson,[3] and Mahsa Ranji[1,*]

[1]*Biophotonics Laboratory, University of Wisconsin Milwaukee, Department of Electrical Engineering and Computer Science, 3200 N Cramer St., Milwaukee, WI 53211-3029, USA*
[2]*Departments of Ophthalmology and Visual Sciences, University of Wisconsin School of Medicine and Public Health, 600 Highland Avenue, Madison, WI, 53792-4673, USA*
[3]*Department of Pediatrics, University of Wisconsin School of Medicine and Public Health, 600 Highland Avenue, Madison, WI, 53792-4673, USA*
**ranji@uwm.edu*

Abstract: Chronic hyperglycemia during diabetes leads to increased production of reactive oxygen species (ROS) and increased oxidative stress (OS). Here we investigated whether changes in the metabolic state can be used as a marker of OS progression in kidneys. We examined redox states of kidneys from diabetic mice, Akita$^{/+}$ and Akita$^{/+}$;TSP1$^{-/-}$ mice (Akita mice lacking thrombospondin-1, TSP1) with increasing duration of diabetes. OS as measured by mitochondrial redox ratio (NADH/FAD) was detectable shortly after the onset of diabetes and further increased with the duration of diabetes. Thus, cryo fluorescence redox imaging was used as a quantitative marker of OS progression in kidneys from diabetic mice and demonstrated that alterations in the oxidative state of kidneys occur during the early stages of diabetes.

OCIS codes: (260.2510) Fluorescence; (000.1430) Biology and medicine; (170.0110) Imaging systems; (170.3880) Medical and biological imaging; (170.6280) Spectroscopy, fluorescence and luminescence; (100.2960) Image analysis.

References and links

1. N. Sheibani, E. A. Scheef, T. A. Dimaio, Y. Wang, S. Kondo, and C. M. Sorenson, "Bcl-2 expression modulates cell adhesion and migration promoting branching of ureteric bud cells," J. Cell. Physiol. **210**(3), 616–625 (2007).
2. J. S. Johansen, A. K. Harris, D. J. Rychly, and A. Ergul, "Oxidative stress and the use of antioxidants in diabetes: linking basic science to clinical practice," Cardiovasc. Diabetol. **4**(1), 5–9999 (2005).
3. L. Piconi, L. Quagliaro, and A. Ceriello, "Oxidative stress in diabetes," Clin. Chem. Lab. Med. **41**(9), 1144–1149 (2003).
4. M. D. Breyer, E. Böttinger, F. C. Brosius 3rd, T. M. Coffman, R. C. Harris, C. W. Heilig, and K. Sharma; AMDCC, "Mouse models of diabetic nephropathy," J. Am. Soc. Nephrol. **16**(1), 27–45 (2005).
5. A. Ceriello, S. Kumar, L. Piconi, K. Esposito, and D. Giugliano, "Simultaneous control of hyperglycemia and oxidative stress normalizes endothelial function in type 1 diabetes," Diabetes Care **30**(3), 649–654 (2007).
6. Y. Ueno, F. Horio, K. Uchida, M. Naito, H. Nomura, Y. Kato, T. Tsuda, S. Toyokuni, and T. Osawa, "Increase in oxidative stress in kidneys of diabetic Akita mice," Biosci. Biotechnol. Biochem. **66**(4), 869–872 (2002).
7. M. M. Delmastro and J. D. Piganelli, "Oxidative stress and redox modulation potential in type 1 diabetes," Clin. Dev. Immunol. **2011**, 593863 (2011).
8. W. I. Sivitz and M. A. Yorek, "Mitochondrial dysfunction in diabetes: from molecular mechanisms to functional significance and therapeutic opportunities," Antioxid. Redox Signal. **12**(4), 537–577 (2010).
9. I. Giardino, D. Edelstein, and M. Brownlee, "Bcl-2 expression or antioxidants prevent hyperglycemia-induced formation of intracellular advanced glycation endproducts in bovine endothelial cells," J. Clin. Invest. **97**(6), 1422–1428 (1996).
10. S. S. Chung, E. C. Ho, K. S. Lam, and S. K. Chung, "Contribution of polyol pathway to diabetes-induced oxidative stress," J. Am. Soc. Nephrol. **14**(Suppl 3), S233–S236 (2003).
11. G. L. King and M. R. Loeken, "Hyperglycemia-induced oxidative stress in diabetic complications," Histochem. Cell Biol. **122**(4), 333–338 (2004).
12. H. Bugger, S. Boudina, X. X. Hu, J. Tuinei, V. G. Zaha, H. A. Theobald, U. J. Yun, A. P. McQueen, B. Wayment, S. E. Litwin, and E. D. Abel, "Type 1 diabetic Akita mouse hearts are insulin sensitive but manifest

#158659 - $15.00 USD Received 23 Nov 2011; revised 16 Dec 2011; accepted 1 Jan 2012; published 10 Jan 2012

structurally abnormal mitochondria that remain coupled despite increased uncoupling protein 3," Diabetes **57**(11), 2924–2932 (2008).
13. B. Chance and G. R. Williams, "A method for the localization of sites for oxidative phosphorylation," Nature **176**(4475), 250–254 (1955).
14. A. Mayevsky, "Brain NADH redox state monitored *in vivo* by fiber optic surface fluorometry," Brain Res. **319**(1), 49–68 (1984).
15. N. Ramanujam, R. Richards-Kortum, S. Thomsen, A. Mahadevan-Jansen, M. Follen, and B. Chance, "Low temperature fluorescence imaging of freeze-trapped human cervical tissues," Opt. Express **8**(6), 335–343 (2001).
16. G. A. Wagnières, W. M. Star, and B. C. Wilson, "*In vivo* fluorescence spectroscopy and imaging for oncological applications," Photochem. Photobiol. **68**(5), 603–632 (1998).
17. R. Richards-Kortum and E. Sevick-Muraca, "Quantitative optical spectroscopy for tissue diagnosis," Annu. Rev. Phys. Chem. **47**(1), 555–606 (1996).
18. M. Ranji, S. Kanemoto, M. Matsubara, M. A. Grosso, J. H. Gorman 3rd, R. C. Gorman, D. L. Jaggard, and B. Chance, "Fluorescence spectroscopy and imaging of myocardial apoptosis," J. Biomed. Opt. **11**(6), 064036 (2006).
19. M. Ranji, M. Matsubara, B. G. Leshnower, R. H. Hinmon, D. L. Jaggard, B. Chance, R. C. Gorman, and J. H. Gorman III, "Quantifying acute myocardial injury using ratiometric fluorometry," IEEE Trans. Biomed. Eng. **56**(5), 1556–1563 (2009).
20. C. H. Barlow, D. A. Rorvik, and J. J. Kelly, "Imaging epicardial oxygen," Ann. Biomed. Eng. **26**(1), 76–85 (1998).
21. S. L. Bernard, J. R. Ewen, C. H. Barlow, J. J. Kelly, S. McKinney, D. A. Frazer, and R. W. Glenny, "High spatial resolution measurements of organ blood flow in small laboratory animals," Am. J. Physiol. Heart Circ. Physiol. **279**(5), H2043–H2052 (2000).
22. C. M. Sorenson, B. J. Padanilam, and M. R. Hammerman, "Abnormal postpartum renal development and cystogenesis in the bcl-2 ($^{-/-}$) mouse," Am. J. Physiol. **271**(1 Pt 2), F184–F193 (1996).
23. Q. Huang, S. J. Wang, C. M. Sorenson, and N. Sheibani, "PEDF-deficient mice exhibit an enhanced rate of retinal vascular expansion and are more sensitive to hyperoxia-mediated vessel obliteration," Exp. Eye Res. **87**(3), 226–241 (2008).
24. E. A. Scheef, Q. Huang, S. Wang, C. M. Sorenson, and N. Sheibani, "Isolation and characterization of corneal endothelial cells from wild type and thrombospondin-1 deficient mice," Mol. Vis. **13**, 1483–1495 (2007).
25. E. A. Scheef, C. M. Sorenson, and N. Sheibani, "Attenuation of proliferation and migration of retinal pericytes in the absence of thrombospondin-1," Am. J. Physiol. Cell Physiol. **296**(4), C724–C734 (2009).
26. J. J. Kelly, J. R. Ewen, S. L. Bernard, R. W. Glenny, and C. H. Barlow, "Regional blood flow measurements from fluorescent microsphere images using an Imaging CryoMicrotome," Rev. Sci. Instrum. **71**(1), 228–234 (2000).
27. B. Chance, B. Schoener, R. Oshino, F. Itshak, and Y. Nakase, "Oxidation-reduction ratio studies of mitochondria in freeze-trapped samples. NADH and flavoprotein fluorescence signals," J. Biol. Chem. **254**(11), 4764–4771 (1979).
28. A. K. Zimmermann, F. A. Loucks, E. K. Schroeder, R. J. Bouchard, K. L. Tyler, and D. A. Linseman, "Glutathione binding to the Bcl-2 homology-3 domain groove: a molecular basis for Bcl-2 antioxidant function at mitochondria," J. Biol. Chem. **282**(40), 29296–29304 (2007).
29. N. Susnow, L. Zeng, D. Margineantu, and D. M. Hockenbery, "Bcl-2 family proteins as regulators of oxidative stress," Semin. Cancer Biol. **19**(1), 42–49 (2009).

1. Introduction

Diabetic nephropathy cases, which have doubled in the past decade, account for approximately half of all end-stage renal disease cases [1–5]. Although oxygen is a necessary component for complex organisms that demand high energy, overproduction of reactive oxygen species (ROS) may cause DNA damage, cell death, and protein modifications that result in mitochondrial and cellular dysfunction [3,6–8]. Diabetes, a common metabolic disorder, can trigger excess generation of ROS and plays an important role in increasing OS oxidative stress (OS) in various tissues, including the kidney. The increased OS during diabetes exacerbates the progression of disease and its associated complications such as renal vascular and proximal tubule dysfunction [1,2,4]. However, the temporal and spatial aspects of these changes and, more specifically, the time of onset of OS during diabetes remain unknown.

The bcl-2 gene plays a central role in maintaining the mitochondrial oxidative homeostasis and its expression is protective during hyperglycemia-induced lipid peroxidation and advanced glycation end product modifications in endothelial cells [9]. Thus, its absence causes a more oxidized state in tissue and, as such, the mitochondria is more oxidized in

#158659 - $15.00 USD Received 23 Nov 2011; revised 16 Dec 2011; accepted 1 Jan 2012; published 10 Jan 2012

bcl-$2^{-/-}$ mice as compared with their controls. In addition, bcl-2 is an anti-apoptotic protein whose expression decreases significantly during diabetes, and thus is of direct interest for this study.

Akita$^{/+}$ mice develop type 1 diabetes as early as 4 weeks of age. Enzymatic and non-enzymatic sources contribute to ROS observed in the diabetic kidneys, including advanced glycation, mitochondrial respiration chain deficiencies, and NAD(P)H oxidase. OS occurs due to the inability of cells to detoxify excess amounts of ROS or loss of the cellular anti-oxidant defense [1,5,10–12]. Thus, the tissue metabolic state is an indicator of cellular oxygen consumption, and it can be extracted from fluorescence images [13,14].

Thrombospondin-1 (TSP1) is a potent endogenous inhibitor of angiogenesis, whose expression is dramatically down regulated during diabetes. Our hypothesis is that decreased production of TSP1 promotes the development and progression of diabetic nephropathy. The Akita$^{/+}$;TSP1$^{-/-}$ mouse is a novel diabetes model developed in Dr. Sheibani's lab that exhibits severe nephropathies with a relatively short duration of diabetes compared with the parental Akita$^{/+}$ mice. Thus, the mice that carry the Akita mutation and lack TSP1 (TSP1$^{-/-}$) serve as a model for severe diabetic nephropathy. Here we propose to determine the impact of the combination of these genetic modifications on the mitochondrial redox state associated with the onset and progression of diabetes. To verify that TSP1$^{-/-}$ genotype itself does not contribute to a more oxidized mitochondria, we compared TSP1$^{-/-}$ mice with Akita$^{/+}$;TSP1$^{-/-}$ mice.

Fluorescence imaging provides specific information on tissue using intrinsic fluorophores or exogenous tagged proteins. Since some of the molecules in the cell have intrinsic fluorophores and are able to fluoresce when excited with the appropriate wavelength, a growing field of fluorescence microscopy techniques relies on autofluorescent fluorophores. Fluorescence-based techniques are widely used in biomedical applications as diagnostic/therapeutic tools for early detection of various diseases such as cancers or heart disease. Optical fluorescence techniques have the potential to diagnose tissue metabolic states in intact organs. These techniques are widely used in biomedical applications and have been shown to have a high sensitivity and specificity for discriminating between diseased and non-diseased tissue [15–17].

Mitochondrial metabolic coenzymes NADH (Nicotinamide Adenine Dinucleotide), and Flavoprotein Adenine Dinocleotide ($FADH_2$) are the primary electron carriers in oxidative phosphorylation. NADH and FAD (the oxidized form of $FADH_2$) are autofluorescent and can be monitored without exogenous labels through the use of optical techniques. These coenzymes are beneficial in that NADH is primarily fluorescent in its reduced biochemical state, whereas FAD is only fluorescent in its oxidized form. Therefore, by imaging these two coenzymes, we can probe the oxidative state of the metabolism in tissue. The fluorescent signals of these intrinsic fluorophores have been used as indicators of tissue metabolism in injuries due to hypoxia, ischemia, and cell death [11,18,19]. In addition, by evaluating the ratio of these two coenzymes, some of the confounding factors in determining this oxidative state can be removed, such as absorbers, including hemoglobin and collagen, as well as scattering effects. Our studies have demonstrated that the normalized ratio of these fluorophores, (NADH/FAD), called the mitochondrial redox ratio (RR), acts as a novel marker of the mitochondrial redox and metabolic state of tissue *ex vivo* and *in vivo*. Although this ratio is not a direct measure of the concentrations of these fluorophores, the fluorescence intensity measured is a relative measure of their concentrations. To date, several groups have used optical fluorescence imaging to probe the biochemical and morphological characteristics of tissues [15,18,20,21]. Here we employed 3D cryo fluorescence redox imaging to delineate the temporal distribution of OS in kidneys from mice with different durations of diabetes.

We have used fluorescent imaging of these two proteins to determine the mitochondrial oxidative state in mice with the above genotypes, resulting in a total of 6 categories of mice, as follows. First, bcl-$2^{-/-}$ mice, which are more sensitive to OS and thus are expected to have

#158659 - $15.00 USD Received 23 Nov 2011; revised 16 Dec 2011; accepted 1 Jan 2012; published 10 Jan 2012

a lower RR, were compared with their bcl-$2^{+/+}$ controls to verify the ability of the system to detect differences in OS. Next, Akita$^{/+}$ and their wild type (WT) controls were studied to determine whether a change in OS is correlated with the presence of diabetes. Similar to bcl-$2^{-/-}$, Akita$^{/+}$ mice are more susceptible to OS and are thus expected to have a lower RR. Finally, Akita$^{/+}$;TSP1$^{-/-}$ mice were compared with their control, TSP1$^{-/-}$, in order to evaluate the severity of diabetic nephropathy in these mice using the mitochondrial oxidative state as a quantitative marker. It should be noted that the name of each group indicates the only modification to the mouse, and thus Akita$^{/+}$, Akita$^{/+}$;TSP1$^{-/-}$ and TSP1$^{-/-}$ are not bcl-2 deficient.

2. Materials and methods

2.1. Tissue preparation

Bcl-2 mice were maintained and screened as previously described [22]. Ins2Akita heterozygous (Akita$^{/+}$) male mice were obtained from Jackson Laboratories, where the colony is maintained by breeding C57BL/6J inbred females with Ins2Akita heterozygous males. Control animals were C57BL/6J male littermates. Only male mice were used in the experiments described below. All diabetic mice were left untreated. All procedures were approved by the Institutional Animal Care and Use Committee of the University of Wisconsin-Milwaukee. Genomic DNA was prepared from tail biopsies and the transgenic Akita$^{/+}$ mice were identified by PCR screening using the following primers: 5′-TGCTGATGCCCTGGCC TGCT-3′ and 5′-TGG TCCCACATATGCACATG-3′. The amplified fragments were digested with FNU 4 HI, as recommended by Jackson Laboratories.

To generate Akita$^{/+}$;TSP1$^{-/-}$ mice, Akita$^{/+}$ male mice were bred with TSP1$^{-/-}$ female mice. The resulting Akita$^{/+}$;TSP1$^{+/-}$ male mice were then bred with TSP1$^{-/-}$ female mice. Akita$^{/+}$;TSP1$^{-/-}$ male mice were determined by screening and the colony was maintained by breeding the respective male mice with TSP1$^{-/-}$ female mice. The litters were screened for Akita$^{/+}$ [23] and TSP1$^{-/-}$ as previously described [24,25].

Here a total of 14 groups of mice (5 mice per group) were studied, as described above. The mice were sacrificed and their kidneys were harvested and frozen rapidly for low temperature cryoimaging. The kidneys were embedded in a black mounting medium and scanned by the cryoimager in 500 slices each 10 μm apart through the whole kidney.

2.2. Cryoimager

Figure 1 shows the schematic for the 3D cryoimager used in this study. The cryoimager is an automated image acquisition and analysis system consisting of software and hardware designed to acquire fluorescence images of tissue sections. A motor-driven microtome sequentially sections frozen tissue at the desired slice thickness while filtered light from a mercury arc lamp excites up to five distinct fluorophores in the exposed surface of the tissue block. The excitation light source is a 200W mercury arc lamp filtered at the excitation wavelength of NADH and FAD, The excitation band pass filters used for NADH is 350 nm (80 nm bandwidth, UV Pass Blacklite, HD Dichroic, Los Angeles, CA) and for FAD is 437 nm (20 nm bandwidth, 440QV21, Omega Optical, Brattleboro, VT) and the emission filters for NADH is 460 nm (50 nm bandwidth, D460/50M, Chroma, Bellows Falls, VT) and for FAD is 537 nm (50 nm bandwidth, QMAX EM 510-560, Omega Optical, Brattleboro, VT). At each slice, a CCD camera records a fluorescence image of the tissue block in pixel dimensions of 10 μm × 10 μm to be later analyzed for fluorophore distribution. The microtome is housed in a freezer unit that maintains the sample at –80°C during sample slicing and image acquisition. The resolution in the z direction of microtome slices can be as small as 5 μm. For this study, we used a resolution of 10 μm in the z direction, which resulted in ~500 z-slices per kidney [21].

#158659 - $15.00 USD Received 23 Nov 2011; revised 16 Dec 2011; accepted 1 Jan 2012; published 10 Jan 2012

2.3. Calibration

A calibration method was designed to compensate for day-to-day variation of light intensity and non-uniformity of the illumination pattern. At the beginning of each experiment and before slicing the tissue, a uniform fluorescent flat plate was placed in the same position as tissue and imaged in all channels to acquire the illumination pattern. Since the fluorescence of the standard is in both the NADH and FAD channels, it also accounts for day-to-day light intensity and uniformity changes in all channels. All the images in each channel were then normalized by dividing each image to the flat plate image, captured in the same channel.

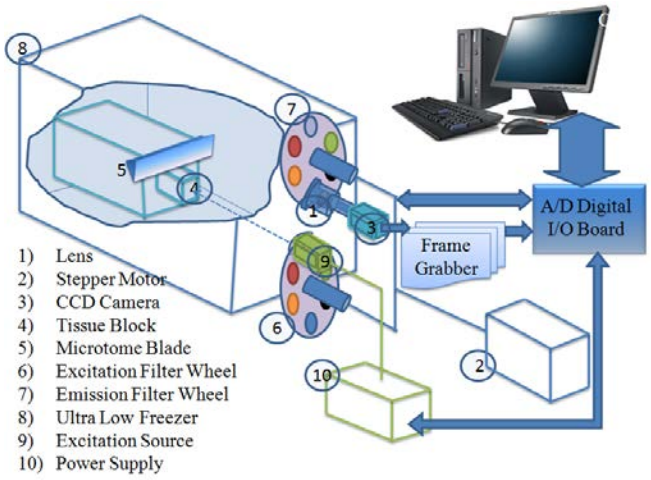

Fig. 1. Schematic of cryoimager [26].

2.4. Data analysis

FAD and NADH autofluorescence images (containing 500 slices per kidney) from each group of kidneys were processed using MATLAB (The MathWorks, Inc., Natick, MA). The composite images were created using all the image slices for each kidney, for both NADH and FAD signals. The ratio of NADH and FAD, known as the mitochondrial redox ratio [27], was calculated voxel by voxel, using Matlab, according to Eq. (1).

$$\text{Redox Ratio} = \text{RR} = \text{NADH} / \text{FAD} \tag{1}$$

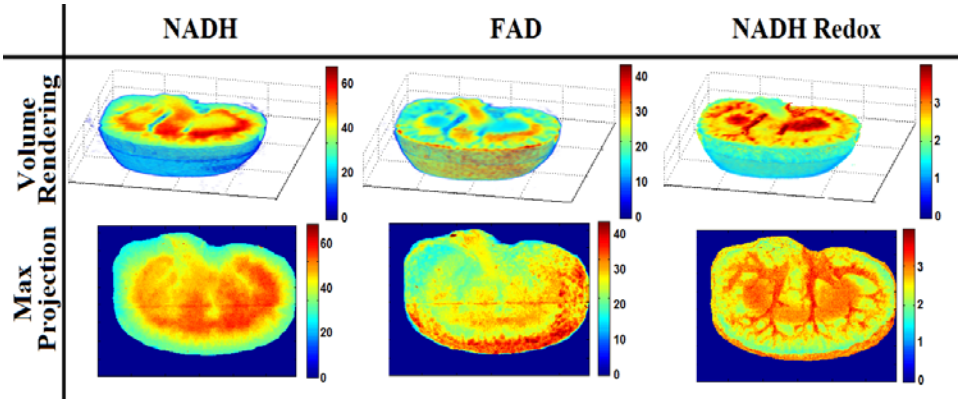

Fig. 2. Images of NADH, FAD and RR for one representative kidney (8 weeks, wild type). The top panel is the result of volume rendering of half of the kidney and the bottom panel is the max projection of the whole volume in the z-axis.

#158659 - $15.00 USD Received 23 Nov 2011; revised 16 Dec 2011; accepted 1 Jan 2012; published 10 Jan 2012

The rendered NADH and FAD images and the redox volume calculation are shown in the first row of Fig. 2. The 2D representation of each kidney was then calculated using the maximum intensities along the z axis of the RR 3D volume (max projection).

In the maximum projection method, first a full 3D volume of images was obtained, including RR, and then the maximum projection on the volumetric data was performed and the histograms were plotted for this maximum projection. The maximum projection is used since the entirety of the anatomy has a significant contribution in this representation. A histogram of the max projection of RR values in each group was created, and the mean (or first moment) of this histogram was calculated according to Eq. (2).

$$Mean = \frac{1}{N_x \times N_y} \sum_{i=1}^{N_x} \sum_{j=1}^{N_y} Kidney\_Maxpro(i, j) \qquad (2)$$

where N_x and N_y are the number of pixels in the x and y directions and the pixel size in x and y is 10μm and 10μm. The previously mentioned histograms were calculated for quantitative comparison between bcl-2, Akita$^{/+}$, and Akita$^{/+}$;TSP1$^{-/-}$ mice and their appropriate controls. Statistical analysis was also carried out for each group of kidneys using a one-tailed student's *t*-test with $P < 0.001$ as the criterion for statistical significance.

3. Results

To ensure that cryo fluorescence redox imaging could effectively measure increased OS in kidney sections we initially examined the RR in kidney sections of wild type (bcl-2$^{+/+}$) and bcl-2-deficient (bcl-2$^{-/-}$) mice. Bcl-2 plays an essential role during kidney development and lack of bcl-2 enhances apoptosis affecting kidney development and growth. Bcl-2$^{-/-}$ mice have a number of defects, including smaller size, and die by six weeks of age from polycystic kidney disease and renal failure. Perhaps more important, bcl-2 plays a central role in maintaining mitochondrial oxidative homeostasis [28] and its deficiency has a significant impact on kidney development and function [9]. In addition, bcl-2 expression is significantly decreased during diabetes [29]. We tested the cryo fluorescence imaging method on kidneys from 3 week-old bcl-2$^{+/+}$ and bcl-2$^{-/-}$ mice. Figure 3 shows the max projected images of NADH, FAD, and RR in bcl-2$^{+/+}$ and bcl-2$^{-/-}$ mice kidneys. The RR indicates a more reduced biochemical state in kidneys from bcl-2$^{+/+}$ mice with a mean value of 2.17 compared with a much smaller mean value of 0.96 in kidneys from bcl-2$^{-/-}$ mice. Thus, kidney sections from bcl-2$^{-/-}$ mice consistently demonstrated increased OS as expected, and are shown in Fig. 3 by a decreased RR (NADH/FAD), confirming the usefulness of this method for measuring OS.

Akita$^{/+}$ mice develop diabetes by 4 weeks of age. We next prepared pseudo color representations of the maximum projection NADH, FAD and RR images and histograms of

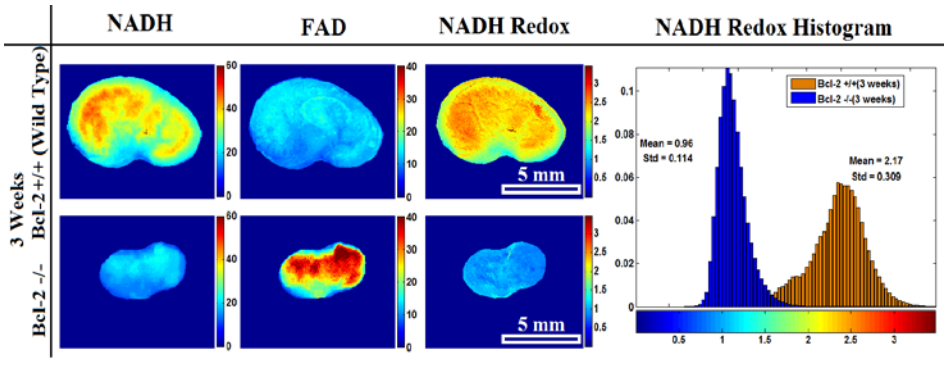

Fig. 3. Representative max projected images of NADH, FAD and RR and their histograms in kidneys from 3 week old bcl-2$^{+/+}$ and bcl-2$^{-/-}$ mice.

#158659 - $15.00 USD Received 23 Nov 2011; revised 16 Dec 2011; accepted 1 Jan 2012; published 10 Jan 2012

the RR for kidneys prepared from 4, 8, and 12 week-old wild-type and Akita$^{/+}$, and 12 week-old TSP1$^{-/-}$ and Akita$^{/+}$;TSP1$^{-/-}$ mice (Fig. 4).

Figure 4 displays, from left to right, images of NADH, FAD, and RR, as well as the RR histogram, for one pair of representative kidneys indicated above. The images show a significant decrease in the mean RR of kidneys from 8 and 12 week-old diabetic mice compared with controls. The RR showed a visible decrease in kidneys from 8 week-old diabetic mice compared with controls, which becomes more significant in kidneys from 12 week-old diabetic mice compared with controls. Thus, these results showed an increase in kidneys' OS with a longer duration of diabetes. The max projected images of Akita$^{/+}$;TSP1$^{-/-}$ and TSP1$^{-/-}$ mice are shown in the last row of Fig. 4. The results presented in the histogram indicate that the mean RR of kidney from 12 week-old Akita$^{/+}$;TSP1$^{-/-}$ mice showed a

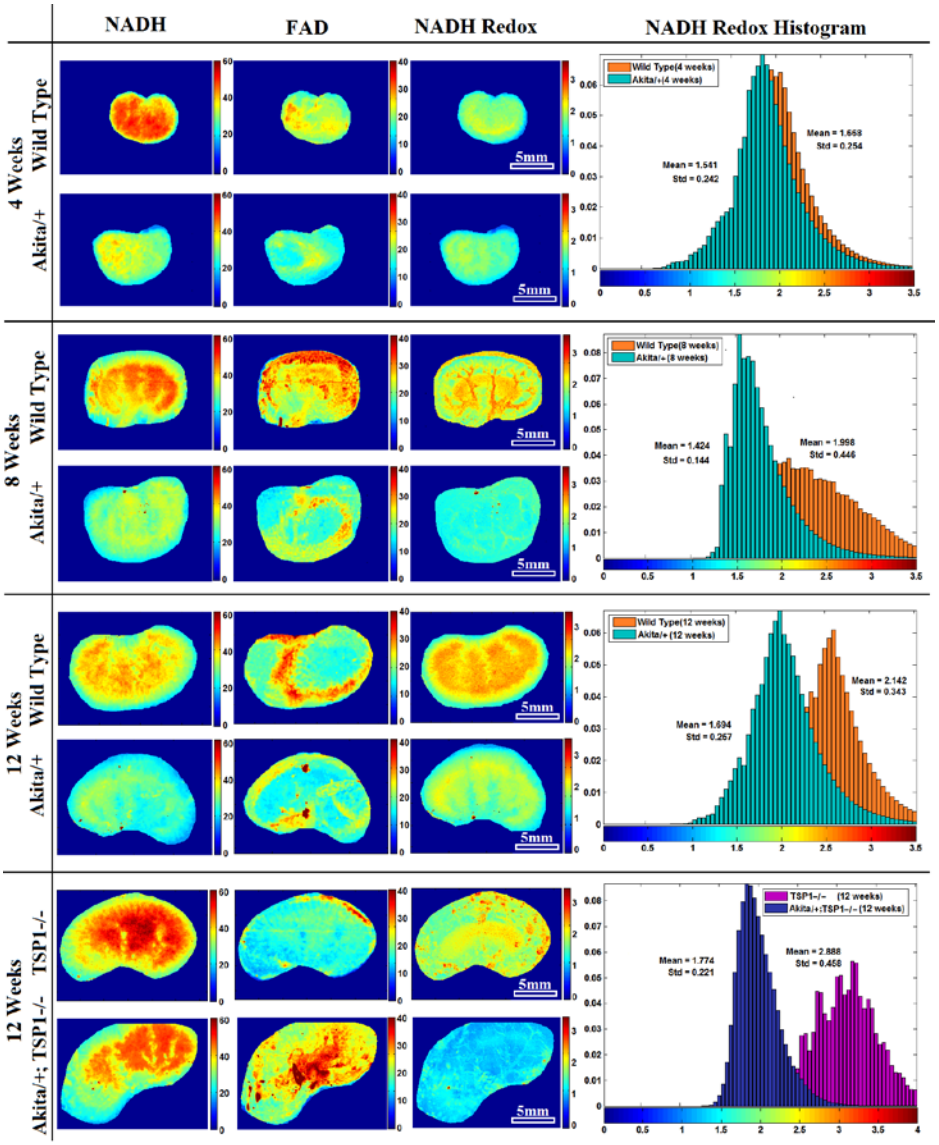

Fig. 4. Representative max projected NADH, FAD and RR images and their related histograms for kidneys from Akita$^{/+}$ and Akita$^{/+}$;TSP1$^{-/-}$ mice and their controls.

#158659 - $15.00 USD Received 23 Nov 2011; revised 16 Dec 2011; accepted 1 Jan 2012; published 10 Jan 2012

more significant decrease compared with control mice, which is a direct result of more OS and severe diabetes complications. These results are consistent with our histological examination of kidneys from these mice, which show more severe diabetic nephropathy.

Figure 5 displays a bar graph plot comparing the mean values of the histograms of max projected images of kidneys from Akita$^{/+}$ and Akita$^{/+}$;TSP1$^{-/-}$ mice versus their appropriate control male littermates. Our results show decreased RR for all Akita$^{/+}$ mice compared with their non-diabetic control littermates.

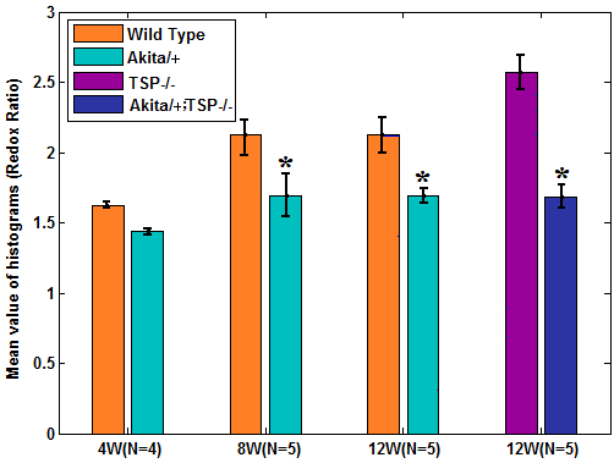

Fig. 5. Bar graph plot comparing the mean values of the histograms of max projected images from Akita$^{/+}$ and Akita$^{/+}$;TSP1$^{-/-}$ mice kidneys and their respective controls. The results show a difference between kidneys from 8 and 12 week-old non-diabetic and diabetic Akita$^{/+}$ mice (*p <0.001). P values were obtained from a one-tailed student's t-test.

4. Discussion and conclusion

In this study, RR was used as a quantitative marker of OS in the kidney. We demonstrated the use of a fluorescence optical imaging technique to delineate temporal distribution of OS during diabetes. We initially confirmed the utility of the methodology in kidneys from bcl-2$^{-/-}$ mice. Bcl-2 is a known modulator of mitochondrial OS and its absence is associated with increased OS state. The RR showed a significant decrease in kidneys from bcl-2$^{-/-}$ mice as compared with their wild-type counterpart. The difference in mean values of the histograms in Fig. 3 suggests that OS shifts the metabolic levels of cells. The result of three groups of diabetic mice and their control littermates demonstrated different redox images and mean values in all three groups and also showed increased OS with the progression of diabetes. Thus, the significant difference in the mean RR of kidneys from diabetic mice compared with their appropriate controls indicates that the sensitivity of RR can be used as a marker of renal OS. Since in the presence of excessive ROS during diabetes mitochondrial coenzymes NADH and $FADH_2$ accumulate in their oxidized forms (NAD and FAD), the mitochondrial RR showed a decrease as a result of OS, as shown in Fig. 5. In the absence of TSP1, diabetes-related damage to the kidney occurred more rapidly, which translated to a further decrease in RR compared with its control littermate (TSP1$^{-/-}$; Fig. 5) and enhanced renal complications. The Akita$^{/+}$ phenotype (diabetic) is key to affecting RR levels. The strong decrease in the mean value of Akita$^{/+}$;TSP1$^{-/-}$ as compared with its control, TSP1$^{-/-}$, combined with the fact that TSP1$^{-/-}$ does not itself decrease the mean value, provides evidence in support of our hypothesis that the lack of TSP1 exacerbates the pathogenesis of diabetic nephropathy.

Our results demonstrate the utility of cryoimaging for measuring kidney tissue mitochondrial redox state in different stages of OS with the progression of diabetes. The RR reveals differences in tissue NADH, FAD, and RR signals between diabetic mice and their control littermates. Furthermore, the studies presented here set the stage for future studies,

#158659 - $15.00 USD Received 23 Nov 2011; revised 16 Dec 2011; accepted 1 Jan 2012; published 10 Jan 2012

using *in vivo* surface fluorescence imaging of mitochondrial signals of kidneys from diabetic mice to follow the progression of diabetes and potentially monitor the efficacy of therapeutic regimens.

Acknowledgments

We appreciate the support of Clinical and Translational Science Institute of Southern Wisconsin grants NIH UL1RR031973 and K12 award (144-PRJ47RG), and UWM RGI grant (101x210). C. M. S. was funded, in part, by the National Institutes of Health (DK067120) and AHA research award (0950057G). N. S. is supported by NIH grants EY016995, EY018179, and RC4 EY 021357 (NS), P30 CA014520 UW, a Paul P. Carbone Cancer Center support grant, P30 EY016665, and an unrestricted departmental award from Research to Prevent Blindness. N. S. is a recipient of a Research Award from American Diabetes Association (1-10-BS-160) and Retina Research Foundation.

#158659 - $15.00 USD Received 23 Nov 2011; revised 16 Dec 2011; accepted 1 Jan 2012; published 10 Jan 2012